Non-linear and anisotropic elastic soft tissue models for medical simulation

Guillaume Picinbono Hervé Delingette Nicholas Ayache

Epidaure Project, INRIA, 06902 Sophia-Antipolis Cedex, BP 93, France
http://www-sop.inria.fr/epidaure/ Hervé.Delingette@sophia.inria.fr

Abstract

In this article, we describe the latest developments of the minimally invasive hepatic surgery simulator prototype developed at INRIA. A key problem with such a simulator is the physical modeling of soft tissues. We propose a new deformable model based on non-linear elasticity and the finite element method. This model is valid for large displacements, which means in particular that it is invariant with respect to rotations. This property improves the realism of the deformations and solves the problems related to the shortcomings of linear elasticity, which is only valid for small displacements. We also address the problem of anisotropic behavior, and volume variations by adding to our model incompressibility constraints. Finally, we demonstrate the relevance of this approach for the real-time simulation of laparoscopic surgical gestures on the liver.

1 Introduction

A major and recent evolution in abdominal surgery has been the development of laparoscopic surgery. In this type of surgery, abdominal operations such as hepatic resection are performed through small incisions. A video camera and special surgical tools are introduced into the abdomen, allowing the surgeon to perform a procedure less invasive. A drawback of this technique lies essentially in the need for more complex gestures and in the loss of direct visual and tactile information. Therefore the surgeon needs to learn and adapt himself to this new type of surgery and in particular to a new type of hand-eye coordination. In this context, surgical simulation systems could be of great help in the training process of surgeons.

Among the several key problems in the development of a surgical simulator [10], the geometrical and physical representation of human organs remain the most important. The deformable model must be at the same time very realistic (both visually and physically) and very efficient to allow real-time deformations. Several methods have been proposed: spring-mass models [3, 9], free form deformations [1], linear elasticity with finite volume method [8] or various finite element methods [6, 7, 12, 4].

In this article we propose a new real-time deformable model based on non-linear elasticity and a finite element method. We first introduce the linear elasticity theory and its implementation through the finite element method, and we then highlight its shortcomings when the "small displacement" hypothesis does not hold. Then we focus on our implementation of St Venant-Kirchhoff elasticity and incompressibility constraints.

2 Shortcomings of the linear elasticity model

Linear elasticity is often used for the modeling of deformable materials, mainly because the equations remain quite simple and the computation time can be optimized.

The physical behavior of soft tissue may be considered as linear elastic if its displacement and deformation remain small [11] (typically less than 10% of the mesh size). We represent the deformation of a volumetric model from its rest shape $\mathcal{M}_{\text{initial}}$ with a *displacement vector* $\mathbf{U}(x, y, z)$ for $(x, y, z) \in \mathcal{M}_{\text{initial}}$ and we write $\mathcal{M}_{\text{deformed}} = \mathcal{M}_{\text{initial}} + \mathbf{U}(x, y, z)$.
From this displacement vector, we define the linearized *Green-St Venant strain tensor* (3×3 symmetric matrix) E_l and its principal invariants l_1 and l_2:

$$E_l = \frac{1}{2}\left(\nabla\mathbf{U} + \nabla\mathbf{U}^t\right), \quad l_1 = tr\, E_l, \quad l_2 = tr\, {E_l}^2. \quad (1)$$

The linear elastic energy W_{Linear}, for homogeneous isotropic materials, is defined by the following formula (see [5]):

$$W_{Linear} = \frac{\lambda}{2}\,(trE_l)^2 + \mu\; tr{E_l}^2 \quad (2)$$

where λ and μ are the *Lamé coefficients* characterizing the material stiffness.

Equation 2, known as *Hooke's law*, shows that the elastic energy of a deformable object is a quadratic function of the displacement vector.

2.1 Finite element method

Finite element method is a classical way to solve continuum mechanics equations. It is a mathematical framework to discretize a continuous variational problem [13]. We chose to use P_1 finite elements where the elementary volume is a tetrahedron with a node defined at each vertex. At each point $\mathbf{M}(x,y,z)$ inside tetrahedron $\mathbf{T}_i$, the displacement vector is expressed as a function of the displacements $\mathbf{U}_k$ of vertices $\mathbf{P}_k$. For P_1 finite elements, interpolation functions Λ_k are linear ($\{\Lambda_k; k=0,...,3\}$ are the barycentric coordinates of $\mathbf{M}$ in the tetrahedron):

$$\mathbf{U}(x,y,z) = \sum_{j=0}^{3} \mathbf{U}_j \Lambda_j(x,y,z)$$

$$\boldsymbol{\Lambda}_j(x,y,z) = \boldsymbol{\alpha}_j.X + \boldsymbol{\beta}_j$$

$$\boldsymbol{\alpha}_j = \frac{(-1)^j}{6V(\mathbf{T}_i)}(\mathbf{P}_{j+1} \times \mathbf{P}_{j+2} + \mathbf{P}_{j+2} \times \mathbf{P}_{j+3} + \mathbf{P}_{j+3} \times \mathbf{P}_{j+1}),$$

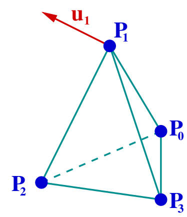

Figure 1: P_1 finite element

where $\times$ stands for the cross product between two vectors, and $V(\mathbf{T}_i)$ is the volume of the tetrahedron.

Using this equation for the displacement vector $\mathbf{U}$ leads to the finite element formulation of linear elastic energy in the tetrahedron $\mathbf{T}_i$ [7]:

$$W_{Elastic}(\mathbf{T}_i) = \sum_{j,k=0}^{3} \mathbf{U}_j^t [\mathcal{B}_{jk}^{\mathbf{T}_i}] \mathbf{U}_k \tag{3}$$

$$\mathcal{B}_{jk}^{\mathbf{T}_i} = \frac{\lambda}{2}(\boldsymbol{\alpha}_j \otimes \boldsymbol{\alpha}_k) + \frac{\mu}{2}\left[(\boldsymbol{\alpha}_k \otimes \boldsymbol{\alpha}_j) + (\boldsymbol{\alpha}_j \ . \ \boldsymbol{\alpha}_k)\, Id_3\right],$$

where $[\mathcal{B}_{jk}^{\mathbf{T}_i}]$ is the tetrahedron contribution to the stiffness tensor of the edge $(\mathbf{P}_j, \mathbf{P}_k)$ (or of the vertex $\mathbf{P}_j$ if $j=k$), $\{\boldsymbol{\alpha}_j, k=0,..,3\}$ are the shape vectors of the tetrahedron and $\otimes$ stands for the tensor product of two vectors.

Finally, to obtain the force $\mathbf{F}_p^{\mathbf{T}_i}$ applied by tetrahedron $\mathbf{T}_i$ on the vertex $\mathbf{P}_p$, we derive the elastic energy with respect to the vertex displacement $\mathbf{U}_p$:

$$\mathbf{F}_p^{\mathbf{T}_i} = 2\sum_{j=0}^{3} [\mathcal{B}_{pj}^{\mathbf{T}_i}] \mathbf{U}_j. \tag{4}$$

We have been using this linear elasticity formulation for several years through two deformable models, the **pre-computed model** [6] and the **tensor-mass model** [7]. Furthermore, it can be extended to anisotropic linear elasticity [12], which allows to model fiber-reinforced materials, very common within biological tissues (tendons, muscles, ...), or other anatomical structures like blood vessels.

2.2 The problem of rotational invariance

The main limitation of the linear model is that it is not invariant with respect to rotations. When the object undergoes a rotation, the elastic energy increases, leading to a variation of the volume (see figure 2). In the case of a global rotation of the object, we could solve the problem with a specific change of the reference frame.

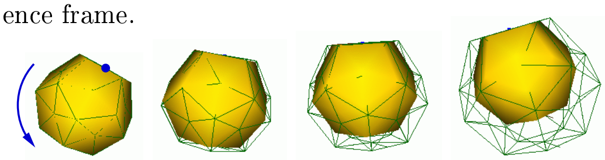

Figure 2: Global rotation of the linear elastic model (wireframe)

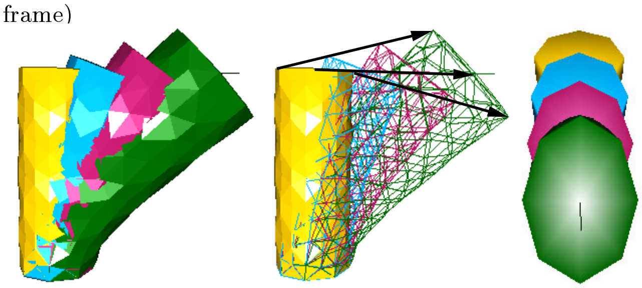

(a) (b) (c)

Figure 3: Successive deformations of a linear elastic cylinder. (a) and (b): side view. (c): top view

But this solution proves itself to be ineffective when only one part of the object undergoes a rotation (which is the case in general). This case is presented by the cylinder of figure 3: the bottom face is fixed and a force is applied to the central top vertex. Arrows show the trajectory of some vertices, which are constrained by the linear model to move along straight lines. This results in the distortion of the mesh. Furthermore, this abnormal deformation is the same in all directions since the object only deforms itself in the rotation plane (figure 3(c)).

This unrealistic behaviour of the linear elastic model for large displacements led us to consider different models of elasticity.

3 St Venant-Kirchhoff elasticity

A model of elasticity is considered as a large displacement model if it derives from a strain tensor which is a quadratic function of the deformation gradient. Most common tensors are the **left** and **right Cauchy-Green strain tensors** (respectively $B = \nabla\phi\nabla\phi^t$ and $C = \nabla\phi^t\nabla\phi$, ϕ being the deformation function).

The St Venant-Kirchhoff model is a generalization of the linear model for large displacements, and is a particular case of hyperelastic materials. The basic energy equation is the same (equation 2), but now E stands for the complete **Green-St Venant strain tensor**:

$$E = \frac{1}{2}(C - I) = \frac{1}{2}\left(\nabla\mathbf{U} + \nabla\mathbf{U}^t + \nabla\mathbf{U}^t\nabla\mathbf{U}\right). \quad (5)$$

Elastic energy, which was a quadratic function of $\nabla\mathbf{U}$ in the linear case, is now a polynomial of order four with respect to $\nabla\mathbf{U}$.

In [12], we have generalized linear elasticity to materials having a different behavior in one given direction. These materials, called "transversally isotropic" materials, can also be modeled with St Venant-Kirchhoff elasticity by adding to the isotropic elastic energy, an anisotropic contribution which penalizes the material stretch in the direction given by unit vector $\mathbf{a}_0$:

$$W_{\text{Trans\_iso}} = W + \left(\frac{\lambda^L - \lambda}{2} + \mu^L - \mu\right)\left(\mathbf{a}_0{}^t\ E\ \mathbf{a}_0\right)^2,$$

where λ^L and μ^L are the Lamé constants along the direction $\mathbf{a}_0$.

3.1 Finite element modeling

With the notations introduced in section 2.1, we express the St Venant-Kirchhoff elastic model with finite element theory as:

$$W(\mathbf{T}_i) = \sum_{j,k} \mathbf{U}_j^t \left[\mathcal{B}_{jk}^{\mathbf{T}_i}\right]\mathbf{U}_k + \sum_{j,k,l}\left(\mathbf{U}_j.\mathcal{C}_{jkl}^{\mathbf{T}_i}\right)(\mathbf{U}_k.\mathbf{U}_l) + \sum_{j,k,l,m} \mathcal{D}_{jklm}^{\mathbf{T}_i}\left(\mathbf{U}_j.\mathbf{U}_k\right)\left(\mathbf{U}_l.\mathbf{U}_m\right), \quad (7)$$

where the terms $\mathcal{B}_{jk}^{\mathbf{T}_i}$, $\mathcal{C}_{jkl}^{\mathbf{T}_i}$, and $\mathcal{D}_{jklm}^{\mathbf{T}_i}$, called stiffness parameters, are given by:

- $\mathcal{B}_{jk}^{\mathbf{T}_i}$ is a (3x3) symmetric matrix:
  $\mathcal{B}_{jk}^{\mathbf{T}_i} = \frac{\lambda}{2}\left(\boldsymbol{\alpha}_j \otimes \boldsymbol{\alpha}_k\right) + \frac{\mu}{2}\left[(\boldsymbol{\alpha}_k \otimes \boldsymbol{\alpha}_j) + (\boldsymbol{\alpha}_j.\boldsymbol{\alpha}_k)\, Id_3\right] + \left(\frac{\lambda^L-\lambda}{2} + \mu^L - \mu\right)(\mathbf{a}_0 \otimes \mathbf{a}_0)(\boldsymbol{\alpha}_j \otimes \boldsymbol{\alpha}_k)(\mathbf{a}_0 \otimes \mathbf{a}_0)$,
- $\mathcal{C}_{jkl}^{\mathbf{T}_i}$ is a vector:
  $\mathcal{C}_{jkl}^{\mathbf{T}_i} = \frac{\lambda}{2}\boldsymbol{\alpha}_j\left(\boldsymbol{\alpha}_k.\boldsymbol{\alpha}_l\right) + \frac{\mu}{2}\left[\boldsymbol{\alpha}_l\left(\boldsymbol{\alpha}_j.\boldsymbol{\alpha}_k\right) + \alpha_k\left(\alpha_j.\boldsymbol{\alpha}_l\right)\right] + \left(\frac{\lambda^L-\lambda}{2} + \mu^L - \mu\right)(\mathbf{a}_0 \otimes \mathbf{a}_0)(\boldsymbol{\alpha}_j \otimes \boldsymbol{\alpha}_k)(\mathbf{a}_0 \otimes \mathbf{a}_0)\boldsymbol{\alpha}_l$,
- and $\mathcal{D}_{jklm}^{\mathbf{T}_i}$ is a scalar:
  $\mathcal{D}_{jklm}^{\mathbf{T}_i} = \frac{\lambda}{8}\left(\boldsymbol{\alpha}_j.\boldsymbol{\alpha}_k\right)\left(\boldsymbol{\alpha}_l.\boldsymbol{\alpha}_m\right) + \frac{\mu}{4}(\boldsymbol{\alpha}_j.\boldsymbol{\alpha}_m)(\boldsymbol{\alpha}_k.\alpha_l) + \left(\frac{\lambda^L-\lambda}{8} + \frac{\mu^L-\mu}{4}\right)(\mathbf{a}_0.\boldsymbol{\alpha}_j)(\mathbf{a}_0.\boldsymbol{\alpha}_k)(\mathbf{a}_0.\boldsymbol{\alpha}_l)(\mathbf{a}_0.\boldsymbol{\alpha}_m)$.

The force applied at each vertex inside a tetrahedron is derived from the elastic energy $W(\mathbf{T}_i)$:

$$\mathbf{F}^p(\mathbf{T}_i) = \underbrace{2\sum_j\left[\mathcal{B}_{pj}^{\mathbf{T}_i}\right]\mathbf{U}_j}_{\mathbf{F}_1^p(\mathbf{T}_i)} + \underbrace{4\sum_{j,k,l}\mathcal{D}_{jklp}^{\mathbf{T}_i}\ \mathbf{U}_l\ \mathbf{U}_k^t\ \mathbf{U}_j}_{\mathbf{F}_3^p(\mathbf{T}_i)} + \underbrace{\sum_{j,k} 2\left(\mathbf{U}_k \otimes \mathbf{U}_j\right)\mathcal{C}_{jkp}^{\mathbf{T}_i} + \left(\mathbf{U}_j.\mathbf{U}_k\right)\mathcal{C}_{pjk}^{\mathbf{T}_i}}_{\mathbf{F}_2^p(\mathbf{T}_i)}. \quad (8)$$

The first term of the elastic force ($\mathbf{F}_1^p(\mathbf{T}_i)$) corresponds to the linear elastic case presented in section 2.1. In the remainder, we deal with the generalization of the tensor-mass model to large displacements.

3.2 Non-linear Tensor-Mass Model

The main idea of the tensor-mass model is to split, for each tetrahedron, the force applied at a vertex in two parts: a force created by the vertex displacement and forces produced by the displacements of its neighbours:

$$\mathbf{F}_1^p(\mathbf{T}_i) = [\mathcal{B}_{pp}^{\mathbf{T}_i}]\mathbf{U}_p + \sum_{j\neq p}[\mathcal{B}_{pj}^{\mathbf{T}_i}]\mathbf{U}_j. \quad (9)$$

This way we can define for each tetrahedron a set of **local stiffness tensors** for vertices ($\{\mathcal{B}_{pp}^{\mathbf{T}_i}; p = 0, ..., 3\}$) and for edges ($\{\mathcal{B}_{pj}^{\mathbf{T}_i}; p, j = 0, ..., 3; p \neq j\}$). By doing this for every tetrahedron, we can accumulate on vertices and edges of the mesh the corresponding contributions to the **global stiffness tensors**:

$$\mathcal{B}_{pp} = \sum_{\mathbf{T}_i \in N(\mathbf{V}_p)} \mathcal{B}_{pp}^{\mathbf{T}_i} \qquad \mathcal{B}_{pj} = \sum_{\mathbf{T}_i \in N(\mathbf{E}_{pj})} \mathcal{B}_{kl}^{\mathbf{T}_i}.$$

These **stiffness tensors** are computed when creating the mesh and are stored for each vertex and edge of the mesh.

The same principle can be applied to the quadratic term ($\mathbf{F}_2^p(\mathbf{T}_i)$ of equation 8) and the cubic term ($\mathbf{F}_3^p(\mathbf{T}_i)$). The former brings **stiffness vectors** for vertices, edges, and triangles, and the latter brings **stiffness scalars** for vertices, edges, triangles, and tetrahedra.

Given a tetrahedral mesh of a solid —in our case an anatomical structure— we build a data structure incorporating the notion of vertices, edges, triangles, and tetrahedra, with all the necessary neighbours. For each vertex, we store its current position $\mathbf{P}_p$, its rest position $\mathbf{P}_p^0$, and its stiffness data. For each edge, we store stiffness data. Finally for each tetrahedron, we store the Lamé coefficients λ and μ, the four shape vectors $\alpha_{\mathbf{k}}$, and the stiffness data.

During the simulation, we compute forces for each vertex, edge, triangle, and tetrahedron, and we use a

Newtonian differential equation to update the vertex positions:

$$m_i \frac{d^2\mathbf{P}_i}{dt^2} = \gamma_i \frac{d\mathbf{P}_i}{dt} + \mathbf{F}_i \qquad (11)$$

This equation is related to the differential equations of continuum mechanics [2]:

$$\mathbf{M}\ddot{\mathbf{U}} + \mathbf{C}\dot{\mathbf{U}} + \mathbf{F}(\mathbf{U}) = \mathbf{R}. \qquad (12)$$

Following finite element theory, the mass $\mathbf{M}$ and damping $\mathbf{C}$ matrices are sparse matrices which are related to the stored physical properties of each tetrahedron. In our case, we consider that $\mathbf{M}$ and $\mathbf{C}$ are diagonal matrices, i.e., that mass and damping effects are concentrated at vertices. This simplification called *mass-lumping* decouples the motion of all nodes and therefore allows us to write equation 12 as the set of independent differential equations for each vertex.

Furthermore, we choose an *explicit integration scheme* where the elastic force is estimated at time t in order to compute the vertex position at time $t+1$:

$$\left(\frac{m_i}{\Delta t^2} - \frac{\gamma_i}{2\Delta t}\right)\mathbf{P}_i^{t+1} = \mathbf{F}_i + \frac{2m_i}{\Delta t^2}\mathbf{P}_i^t - \left(\frac{m_i}{\Delta t^2} + \frac{\gamma_i}{2\Delta t}\right)\mathbf{P}_i^{t-1}.$$

One of the basic tasks in surgery simulation consists in cutting soft tissue. With our deformable model, this task can be achieved efficiently. We simulate the action of an electric scalpel on soft tissue by successively removing tetrahedra at places where the instrument is in contact with the anatomical model.

When removing a tetrahedron, 280 floating numbers update operations are performed to suppress the tetrahedron contributions to the stiffness data of the surrounding vertices, edges, and triangles. By locally updating stiffness data, the tissue has exactly the same properties as if we had removed the corresponding tetrahedron at its rest position. Because of the volumetric continuity of finite element modeling, the tissue deformation remains realistic during the cutting.

4 Incompressibility constraint

Living tissue, which is essentially made of water, is nearly incompressible. This property is difficult to model and leads in most cases to instability problems. This is the case with the St Venant-Kirchhoff model: the material remains incompressible when the Lamé constant λ tends towards infinity. Taking a large value for λ would force us to decrease the time step and therefore to increase the computation time. Another reason to add an external incompressibility constraint to our model is related to the model itself: the main advantage of the St Venant-Kirchhoff model is to use the strain tensor E which is invariant with respect to rotations. But it is also invariant with respect to symmetries, which could lead to the reversal of some tetrahedra under strong constraints.

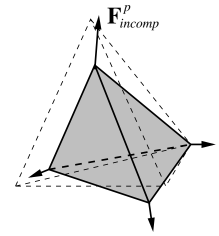

Figure 4: Penalization of the volume variation

We choose to penalize volume variation by applying to each vertex of the tetrahedron a force directed along the normal of the opposite face $\mathbf{N}_p$ (see figure on the right), the norm of the force being the square of the relative volume variation:

$$\mathbf{F}^p_{incomp} = \left(\frac{V - V_0}{V_0}\right)^2 \vec{\mathbf{N}}_p.$$

These forces act as a pressure increase inside the tetrahedron. This method is closely related to Lagrange multipliers, which are often used to solve problem of energy minimization under constraints.

5 Results

In the first experiment, we wish to highlight the contributions of our new deformable model in the case of partial rotations. Figure 5 shows the same experience as the one presented for linear elasticity (section 2.2, figure 3). On the left we can see that the cylinder vertices can now follow trajectories different from straight lines (figure 5(a)), leading to much more realistic deformations than in the linear (wire-frame) case (figures 5(b) and 5(c)).

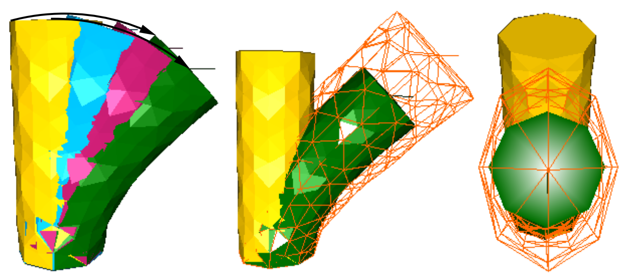

Figure 5: Non-linear (solid rendering) v. linear model (wireframe)

The second example presents the differences between isotropic and anisotropic materials. The three cylinders of figure 6 have their top and bottom faces fixed, and are submited to the same forces. While the isotropic model on the left undergoes a "snake-like" deformation, the last two, which are anisotropic along their height, stiffen in order to minimize their stretch in the anisotropic direction. The rightmost model, being twice as stiff as the other in the anisotropic direction, starts to squeeze in the plane of isotropy because it can not stretch anymore.

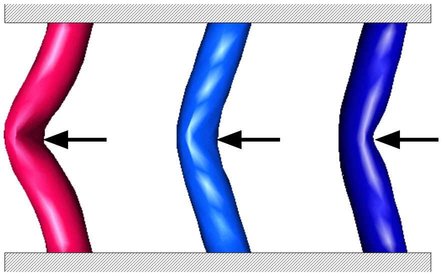

Figure 6: Deformation of tubular structures with non-linear transversally isotropic elasticity.

In the third example (figure 7), we apply a force to the right lobe of the liver (the liver is fixed in a region near the center of its back side, and Lamé constants are: $\lambda = 4.10^4 kg/cm^2$ and $\mu = 10^4 kg/cm^2$). Using the linear model, the right part of the liver undergoes a large (and unrealistic) volume increase, whereas with non-linear elasticity, the right lobe is able to partially rotate, while undergoing a much more realistic deformation.

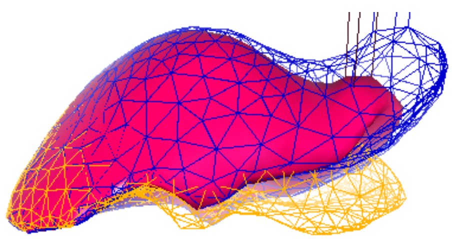

Figure 7: Linear (wireframe), non-linear (solid) liver models, and rest shape (bottom)

Adding the incompressibility constraint on the same examples decreases the volume variation even more (see table 1), and also stabilizes the behaviour of the deformable models in strongly constrained areas.

Volume variations (%)	Linear	Non linear	Non linear incomp.
Cylinder			
left	7	0.3	0.2
middle	28	1	0.5
right	63	2	1
Liver	9	1.5	0.7

Table 1: Volume variation results. For the cylinder: left, middle and right stand for the different deformations of figures 3 and 5(a)

The last example is the simulation of a typical laparoscopic surgical gesture on the liver. One tool is pulling the edge of the liver sideways while a bipolar cautery device cuts it. During the cutting, the surgeon pulls away the part of the liver he wants to remove. This piece of liver undergoes large displacements and the deformation appears fairly realistic with this new non-linear deformable model (figure 8).

Obviously, the computation time of this model is larger than for the linear model because the force equation is much more complex (equation 8). With our current implementation, simulation frequency is five times slower than with the linear model. Nevertheless, with this non-linear model, we can reach a frequency update of 25 Hz on meshes made of about 2000 tetrahedra (on a PC Pentium PIII 500M Hz). This is sufficient to reach visual real-time with quite complex objects, and even to provide a realistic haptic feedback using force extrapolation as described in [12].

6 Optimization of non-linear deformations

We have shown in this article that non-linear elasticity allows to simulate much more realistic deformations than linear elasticity as soon as the model undergoes large displacements. However, non-linear elasticity is more computationally expensive than linear elasticity. Since, non-linear elastic forces are equal to linear elastic forces as the maximum vertex displacement decreases to zero, we propose to use non-linear elasticity only at parts of the mesh where displacements are larger than a given threshold, the remaining part using linear elasticity.

Figure 9 shows a deformation computed with this optimization (same experiment as in figure 7). The threshold is set to 2 cm while the liver mesh is about 30 cm long. The points drawn on the surface identify vertices using non-linear elasticity. With this method, we reach an update frequency of 20 Hz instead of 8 Hz with a fully non-linear model.

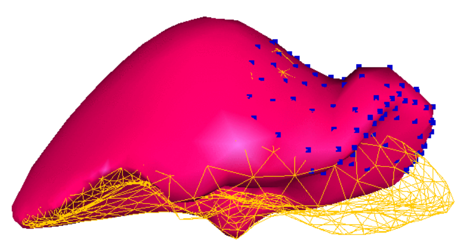

Figure 9: Adaptative non-linear model deformation compared with its rest position (wire-frame)

The diagram below shows the update frequencies reached for several value of the threshold.

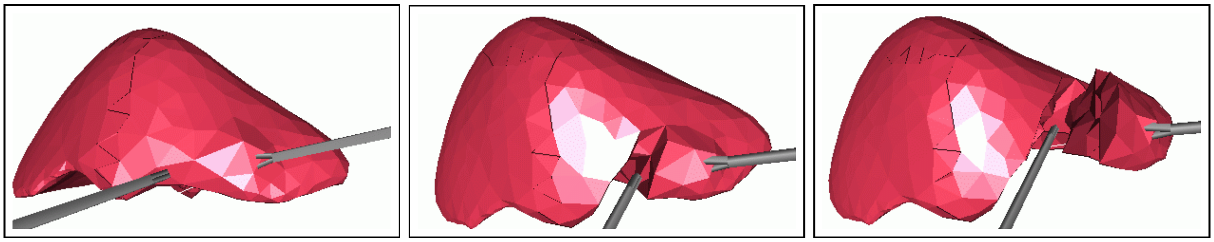

Figure 8: Simulation of laparoscopic liver surgery

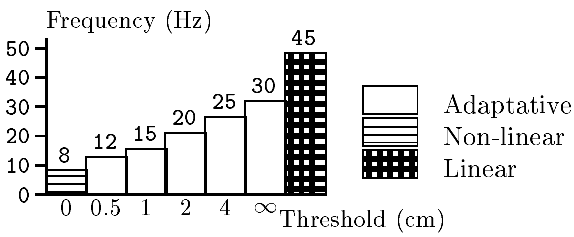

For the simulation example of figure 8, this optimization allows to reach update frequencies between 50 and 80 Hz, depending on the ratio of points using non-linear elasticity. The minimal frequency of 50 Hz is reached at the end of the simulation, when all vertices of the resected part of the liver are using large displacement elasticity (figure 10).

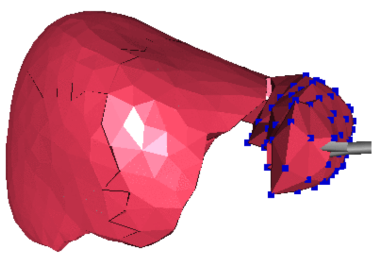

Figure 10: Surgery simulation using adaptative model

7 Conclusion

We have proposed in this article a new deformable model based on large displacement elasticity, anisotropic behavior, finite element method, and a dynamic explicit integration scheme. It solves the problem of rotational invariance of deformations and takes into account the incompressibility properties of biological tissues. Including this model into our laparoscopic surgery simulator prototype improves its biomechanical realism and thus increases its impact in the learning and training processes.

References

[1] C. Basdogan, C. Ho, M. A. Srinivasan, S. D. Small, and S. L. Dawson. Force Interaction in Laparoscopic Simulation: Haptic Rendering Soft Tissues. In *MMVR'6*, pages 28–31, San Diego CA, january 1998.

[2] K.-L. Bathe. *Finite Element Procedures in Engineering Analysis*. Prentice-Hall, 1982.

[3] F. Boux de Casson and C. Laugier. Modeling the Dynamics of a Human Liver for a Minimally Invasive Surgery Simulator. In *MICCAI'99*, pages 1156–1165, Cambridge UK, 1999.

[4] Morten Bro-Nielsen and Stephane Cotin. Real-time Volumetric Deformable Models for Surgery Simulation using Finite Elements and Condensation. In *Eurographics '96. ISSN 1067-7055*, pages 57–66. Blackwell Publishers, 1996.

[5] P. G. Ciarlet. *Mathematical elasticity Vol. 1: Three-dimensional elasticity*. Elsevier Science Publishers B.V., 1988.

[6] S. Cotin, H. Delingette, and N. Ayache. Real-time elastic deformations of soft tissues for surgery simulation. *IEEE Transactions On Visualization and Computer Graphics*, 5(1):62–73, January-March 1999.

[7] S. Cotin, H. Delingette, and N. Ayache. A Hybrid Elastic Model for Real-Time Cutting, Deformations and Force Feedback for Surgery Training and Simulation. *The Visual Computer*, 16(8):437–452, 2000. Also available as INRIA research report RR-3510.

[8] G. Debunne, M. Desbrun, A. Barr, and M.-P. Cani. Interactive multiresolution animation of deformable models. In *CAS'99*, September 1999.

[9] D. Lamy and C. Chaillou. Design, Implementation and Evaluation of an Haptic Interface for Surgical Gestures Training. In *International Scientific Workshop on Virtual Reality and Prototyping*, pages 107–116, Laval, France, June 1999.

[10] J. Marescaux, J-M. Clément, V. Tassetti, C. Koehl, S. Cotin, Y. Russier, D. Mutter, H. Delingette, and N. Ayache. Virtual Reality Applied to Hepatic Surgery Simulation: The Next Revolution. *Annals of Surgery*, 228(5):627–634, 1998.

[11] W. Maurel, Y. Wu, N. M. Thalmann, and D. Thalmann. *Biomechanical Models for Soft Tissue Simulation*. Springer-Verlag, 1998.

[12] G. Picinbono, J.C. Lombardo, H. Delingette, and N. Ayache. Improving Realism of a Surgery Simulator: Linear Anisotropic Elasticity, Complex Interactions and Force Extrapolation. *The Journal of Visualization and Computer Animation*, 2001. accepted (also available as INRIA research report RR-4018).

[13] O. Zienkiewicz. *The finite element method*. Mc Graw-Hill, London, 3^{rd} edition, 1977.